Journal of Applied Polymer Science

The Cell Forming Process of Microcellular Injection-Molded Parts

Guiwei Dong,[1] Guoqun Zhao,[1] Yanjin Guan,[1] Guilong Wang,[1] Xiaoxin Wang[1,2]
[1]Key Laboratory for Liquid-Solid Structural Evolution and Processing of Materials (Ministry of Education), School of material Science & Engineering, Shandong University, Jinan, Shandong 250061, People's Republic of China
[2]Qingdao Hisense Mould Co., Ltd., Qingdao Shandong 266114, People's Republic of China
Correspondence to: G. Zhao (E-mail: zhaogq@sdu.edu.cn)

ABSTRACT: In this article, we studied the cell forming process of microcellular injection-molded parts. Using a modified injection molding machine equipped with a Mucell® SCF delivery system, microcellular-foamed acrylonitrile–butadiene–styrene parts with different shot sizes were molded. The cell structure on the fractured surfaces along the direction both vertical and parallel to melt flow in the molded parts was examined. The results showed that a regular spherical cells region and a distorted ellipsoidal cells region exist in the molded parts simultaneously. The length of the distorted cells region along the melt flow direction in the molded parts remained basically unchanged for different shot sizes and it is about 195 mm away from the flow front in this study's conditions. The cell formation mechanism was analyzed, two cell forming processes in microcellular injection molding, the "foam during filling" process and the "foam after filling" process, were proposed. It was also found that the melt pressure in the filling stage is the dominant factor affecting the cell forming process, and there is a critical melt pressure value in the filling stage, 20.9 MPa, as the dividing line of the two cell forming processes in this study. © 2014 Wiley Periodicals, Inc. J. Appl. Polym. Sci. **2014**, *131*, 40365.

KEYWORDS: foams; morphology; molding

Received 15 September 2013; accepted 30 December 2013
DOI: 10.1002/app.40365

INTRODUCTION

Microcellular plastics were developed at MIT by Martini and his colleagues in 1980s with an effort to reduce the amount of material used by creating a large number of small cells without significantly compromising the mechanical properties.[1,2] Compared with the conventional foamed polymers, microcellular plastics have a larger number of tiny cells that are even smaller than the critical flaws (cracks) that pre-exist in the polymer. Hence, the micron-sized cells formed in the polymer matrix may serve as crack arrestors by blunting crack tips, thereby enhancing the part toughness, impact strength, and fatigue life.[3–5] Thus, as the concept of the microcellular plastics was proposed, it has been attracted significant attention from the polymer association and led to the development of various microcellular foaming techniques such as batch foaming,[6] thermoforming,[7] extrusion,[8,9] and injection molding.[10–13] Among them, the microcellular injection molding process is one of the most promising methods and was first commercialized by Trexel Inc. under the Mucell name.

Figure 1 shows the scanning electron microscope (SEM) image of a typical fracture surface in microcellular parts produced by microcellular injection molding process in this study. It can be seen that two different regions, the foamed core and the unfoamed skins, exist on the fractured surface, which form a special sandwich-like structure within the molded parts. This is the most typical characteristics of microcellular injection-molded parts. According to the previous studies, the cell structure has a critical influence on the physical and mechanical properties of microcellular injection-molded parts.[14–16] The smaller the size of the cells is and the more uniform the cell distribution is, the higher the mechanical properties, such as tensile and bending strength, of the microcellular molded part are. Thus, research on the cell structure and morphology in microcellular injection-molded parts has always been a hotspot and many studies have been done in this field.

In the aspect of cell structure researches, Behravesh and Rajabpour[17] carried out an experimental research on the filling stage of microcellular injection molding process and found that the shot size has a dominant effect on foam or cell structure, too low a shot size causes a nonuniform microstructure and incompletely foamed part, and at too high a shot size, the gas will remain dissolved in the polymer matrix. The similar results was found by Yuan et al.,[18] they studied the microcellular injection molding of polyamide-6 nanocomposites, proposed that the shot size appears to be the most predominant molding parameter affecting the cell size and cell density; whereas, for the same part with the same shot size, Rezavand et al.[19] found that cell size, cell distribution, and skin thickness are different at various

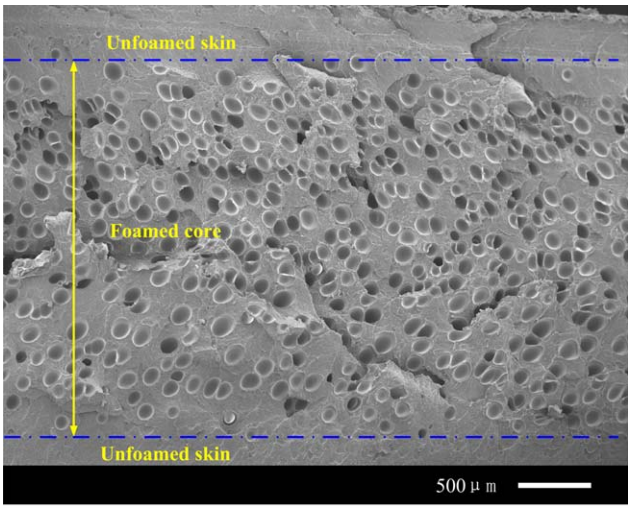

Figure 1. SEM image of typical fracture surface in microcellular injection-molded parts. [Color figure can be viewed in the online issue, which is available at wileyonlinelibrary.com.]

regions. For microcellular injection-molded nanocomposites, Hwang et al.[20,21] recently found that the cell size decreased as the clay loading increased in microcellular thermoplastic olefin elastomers (TPO)–clay nanocomposites and ethylene vinyl acetate (EVA)–clay nanocomposites.

All of the above studies showed that it is not an easy work to obtain an ideal cell structure in microcellular injection molding, and many efforts have been made in the cell structure control technology. Leicher et al.[22] investigated the influence of key processing parameters on the morphology of the microcellular injection-molded porous structures. It is concluded that the increase of the injection speed and the decrease of the polymer melt temperature will decrease the pore or cell sizes, whereas the increase in the degree of weight reduction will increase the pore or cell sizes. Using an independently developed microcellular injection molding equipment, Huang and Wang[23] studied the effects of the nozzle temperature, injection speed, and shot size on the cellular structure and skin layer thickness of the microcellular injection-molded tensile specimen of polystyrene material. The results showed that fine and uniform cell structure is formed when the nozzle temperature is between 165 and 180°C. With the increase of the injection speed or shot size, the cell diameter decreases, the cell density increases, and the cellular structure uniformity is improved. Recently, Gomez et al.[24] investigated the effect of injection molding parameters on the foam morphology of microcellular-molded ethylene-propylene block copolymer (EPBC) parts and found that low shot volume produces uniform density cellular structures and larger cores, whereas lower mold temperatures help maintain small cell sizes.

However, there have been a lot of studies on the cell structure and its control technology in microcellular injection-molded parts. Through comprehensive analysis, it can be found that the existing studies mainly focused on the final cell structure of the microcellular injection-molded parts. The research on the cell forming process of microcellular injection-molded parts was usually ignored, and there was no relevant analysis about the final cell structure and the cell forming processes. On the other hand, most of the current investigations on the cell structure in microcellular injection-molded parts examined only the fracture surfaces vertical to melt flow direction. There are few comparative studies about the cell structure on the fracture surfaces parallel to melt flow direction so as to lead the results about the cell morphology to be one sided. Indeed, the microcellular injection molding is an extremely complex technological process, and hence different cell structures may result from different cell forming processes. Studying the cell forming process has great theoretical and practical significance for understanding the microcellular injection molding process.

This article systematically performs an experimental investigation on the microcellular injection molding process under different shot size conditions, which represent the different stages of the filling process in microcellular injection molding, respectively. The cell structures on the fracture surfaces both vertical and parallel to melt flow direction in the molded parts are examined and studied. The cell formation mechanism of microcellular injection molding is discussed. Two cell forming processes, the "foam during filling" process and the "foam after filling" process, dominated by a critical melt pressure in microcellular injection molding were proposed.

EXPERIMENTAL

Material

The polymer material used in this study was acrylonitrile–butadiene–styrene (ABS) copolymer (HF380, LG Chemical, Korea). Its melt flow index is 43 g/min at 230°C and its density at room temperature is 1.04 g/cm^3. Before injection processing, the material was dried at 80°C for 4 h to remove moisture.

Part Geometry

A medical device front cover with dimensions of 510 mm (length) × 320 mm (width) × 70 mm (height) and a wall thickness of 3 mm was used for the experiments of microcellular injection molding process in this study. Figure 2 shows the

Figure 2. The injected microcellular part of a medical device front cover. [Color figure can be viewed in the online issue, which is available at wileyonlinelibrary.com.]

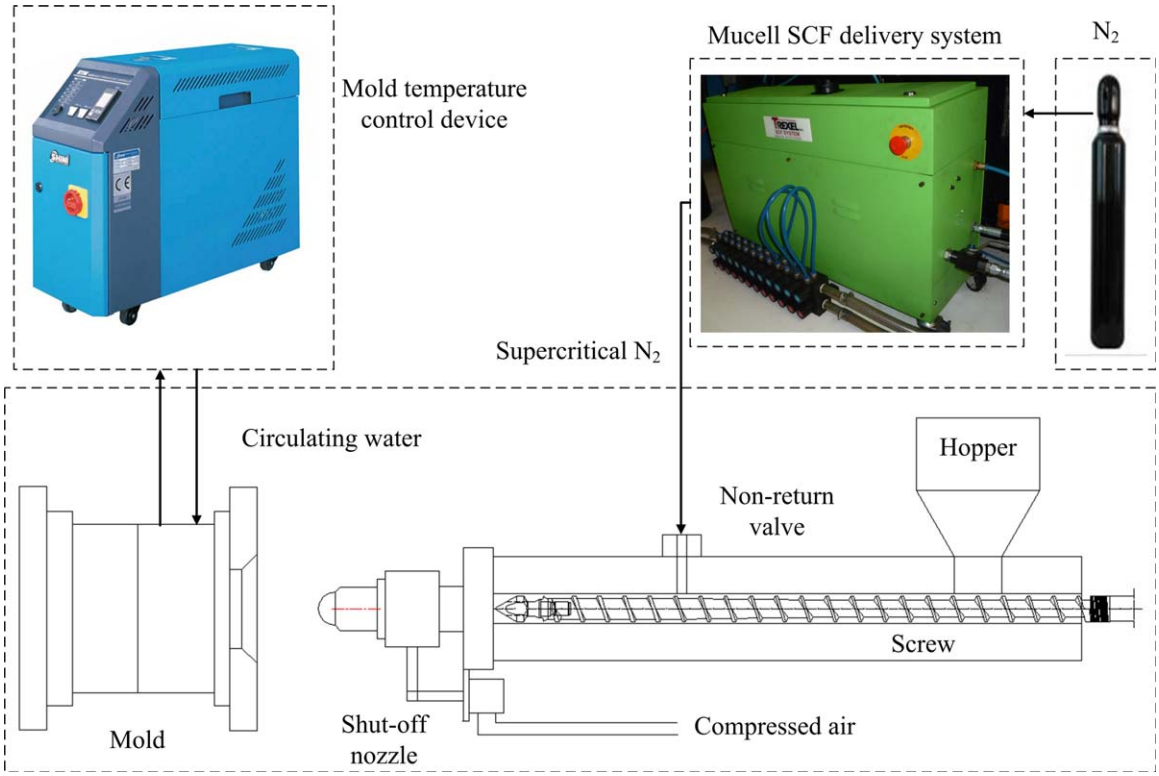

Figure 3. Schematic representation of the microcellular injection molding equipment used in this study. [Color figure can be viewed in the online issue, which is available at wileyonlinelibrary.com.]

injected microcellular part of the medical device front cover. The front side of the part is shown in Figure 2(a), and the back side of the part and the gate location are shown in Figure 2(b).

Injection Molding Machine

The injection molding machine used for microcellular injection molding process was Borch BS800-III (Guangzhou, China), equipped with a Mucell SCF delivery system (Trexel, United States), a shut-off nozzle (Herzog, Switzerland), and a mold temperature control device (Shini, China). The injection molding machine has a clamping force of 8000 kN, the maximum injection pressure is 2090 bar, and the screw diameter is 100 mm with an *L*/*D* ratio of 22 : 1. Nitrogen was used as the physical blowing agent. The schematic representation of the microcellular injection molding equipment used in this study is shown in Figure 3.

Experimental Setup

To investigate the cell forming process in microcellular injection molding, this article selected the microcellular injection-molded parts with different shot sizes as the study and examination objects, which represent the different moments of the filling stage in microcellular injection molding, respectively. The screw injection displacement is taken as a measurement standard of the shot size. Through several experimental adjustments, it is found that when shot size is 120 mm, the part just completely fills the mold cavity and no short shot occurs exactly. Therefore, the shot size of 120 mm can be selected as the set value of the shot volume of 100%.

After the microcellular injection molding process runs steadily, the molded parts with shot sizes of 24, 48, 72, 96, and 120 mm are chosen as the studied and examined parts. These above five levels of the shot sizes correspond to the shot volume percentages of 20, 40, 60, 80, and 100%, respectively. Table I summarizes the processing conditions for the microcellular injection molding process in this study. Figure 4 shows the microcellular injection-molded parts with different shot sizes obtained in this experiment.

Preparation of Samples

For each of the microcellular injection-molded parts with different shot sizes obtained in this study, a strip with width of 20 mm was cut out along the melt flow direction from the gate position. Then, for each strip, experimental observation samples with a dimension of 20 mm × 8 mm were cut out at an interval of 50 mm from the gate. All of the samples were fractured in liquid nitrogen. The fractured surface of every sample was

Table I. Experimental Conditions for the Microcellular Injection Molding

Injection speed (mm/s)	44
SCF percentage (%)	0.4
Melt temperature (°C)	240
Mold temperature (°C)	45
Back pressure (bar)	20
Cooling times (s)	20
Packing times (s)	0
Shot size (mm)	24, 48, 72, 96, and 120

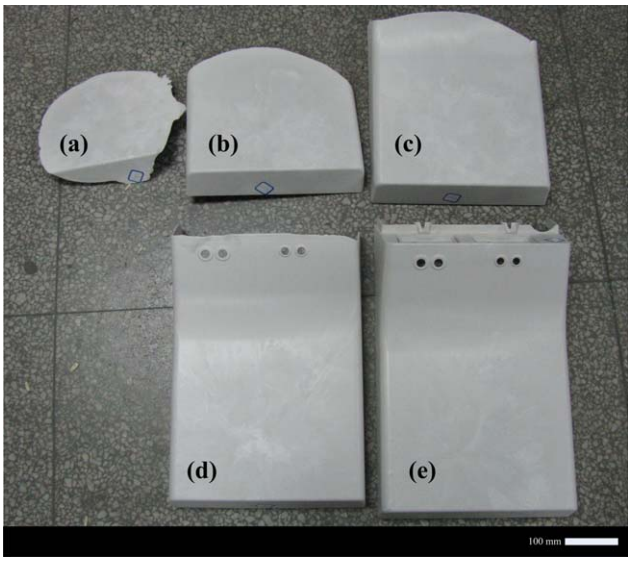

Figure 4. Microcellular injection-molded parts with different shot sizes: (a) 24 mm; (b) 48 mm; (c) 72 mm; (d) 96 mm; and (e) 120mm. [Color figure can be viewed in the online issue, which is available at wileyonlinelibrary.com.]

coated with an approximately 10-nm thick layer of gold and observed with a JEOL JSM-6610LV SEM.

To comprehensively examine the cell structure in the molded parts, the SEM samples were taken on the cross-sections both vertical and parallel to melt flow direction. Figure 5 shows the SEM sample taking positions, where the shadow surfaces on the samples are the observed surfaces. For the gate position of each strip in microcellular injection-molded parts with different shot sizes, the SEM samples are taken only vertical to melt flow direction, which correspond to the cell structure to be observed is that on the fractured surface parallel to melt flow direction. In other positions of each strip in the parts with different shot sizes, the SEM samples are taken vertical and parallel, respectively, to melt flow direction. Correspondingly, the cell structures to be observed are those on the fractured surfaces parallel and vertical, respectively, to melt flow direction.

RESULTS AND DISCUSSION

Cell Structure

Taking the microcellular injection-molded part with the shot size of 72 mm as a representative, the cell structures on the fracture surfaces are shown in Figure 6. Figure 6(a–d) shows the cell structure in the positions of 50, 100, 150, and 200 mm away from the gate; labels v and p, respectively, denote the direction vertical and parallel to melt flow direction.

As shown in Figure 6(a-v,a-p), it can be seen that in the positions near the gate, there is little difference between the morphology of the cell structure vertical and the parallel to melt flow direction. The shape of the cells is near-spherical and the distribution of cell sizes is relatively uniform. But in the positions far from the gate, the morphology of cell structures vertical and parallel to melt flow direction has significant difference. Along vertical to melt flow direction, the shape of the cells is still near-spherical as shown in Figure 6(b-v,c-v). While the distribution of cell sizes becomes more nonuniform as the distance away from the gate becomes larger, and there even appears huge cells with the diameter of 300 μm in the position near the flow front as shown in Figure 6(d-v). Overall, although the cell sizes distribute unevenly along vertical to melt flow direction, the shape of the cells was basically near-spherical and without obvious deformation.

However, along parallel to melt flow direction in the positions far from the gate, the shape of the cells has a distinct deformation. Except the cells in the central line of the cross-section is spherical like, the cells in both sides of the central line are distorted into spindly ellipsoids as shown in Figure 6(c-p). It also can be seen that with the increase of the distance from the gate, the distortion of the cells on the cross-section parallel to melt flow direction increases. Especially in the position near the melt

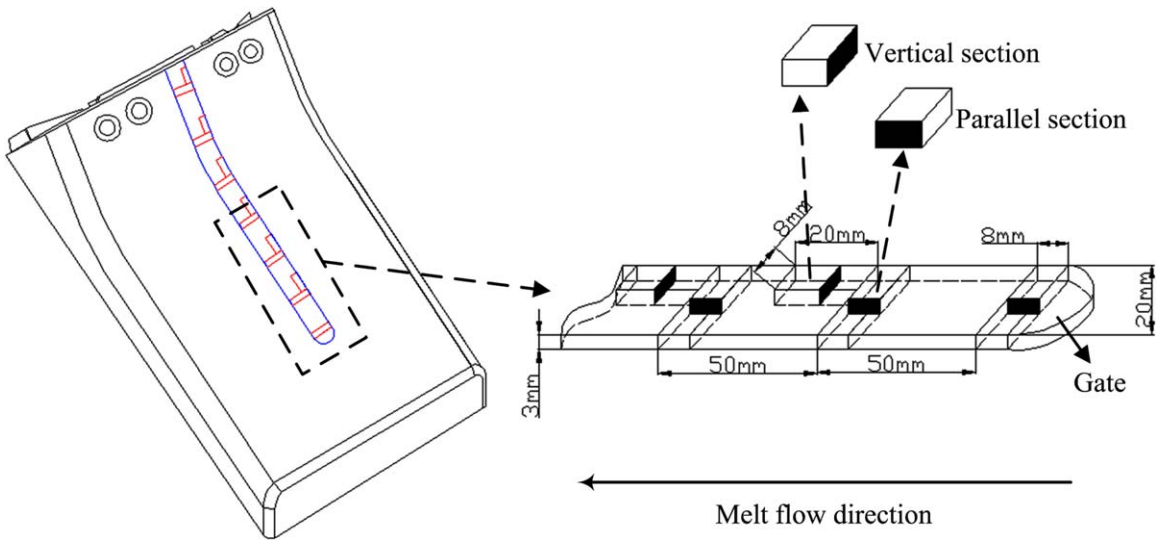

Figure 5. Schematic representation of SEM sample preparation. [Color figure can be viewed in the online issue, which is available at wileyonlinelibrary.com.]

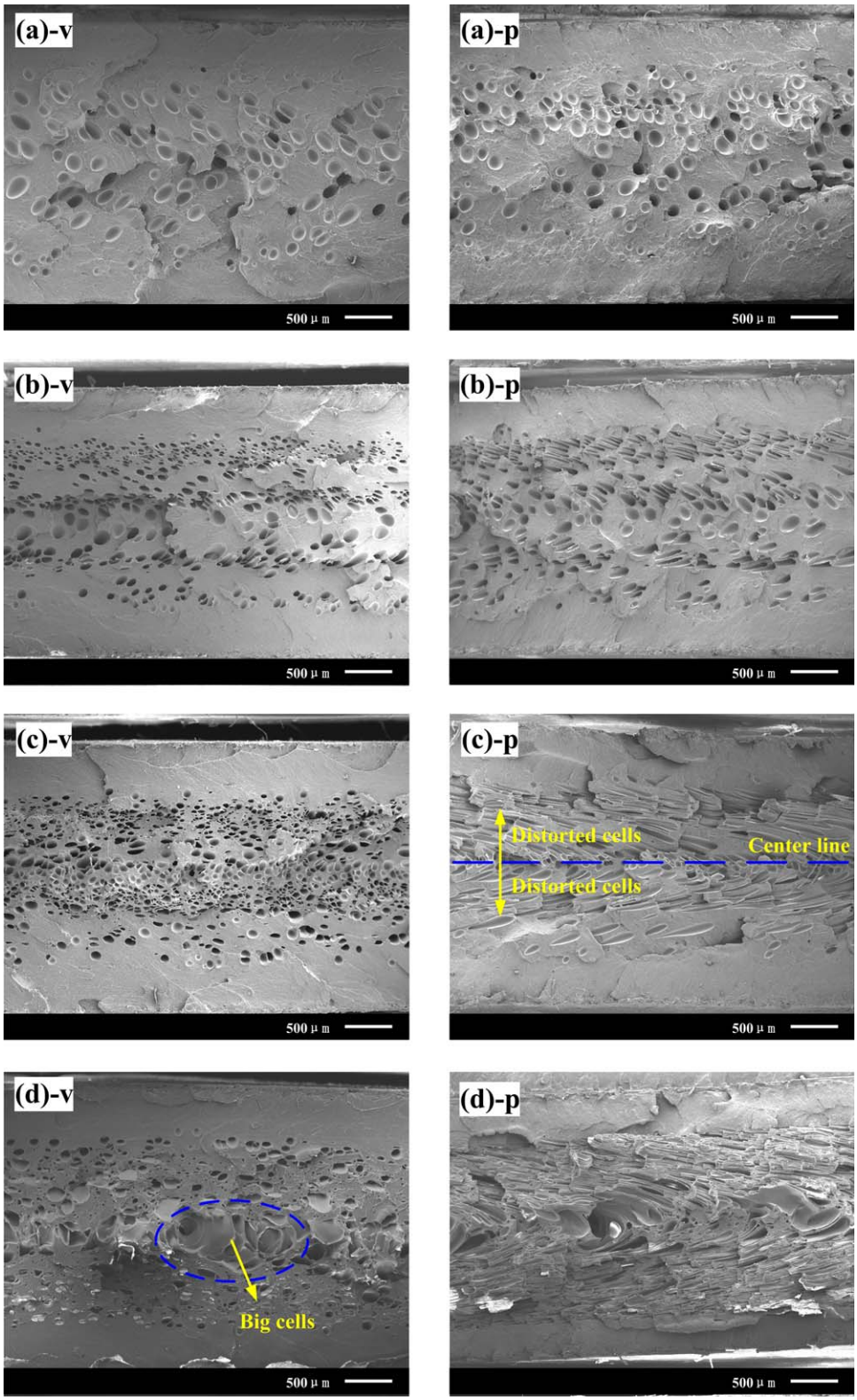

Figure 6. SEM micrographs of microcellular injection-molded part with the shot size of 72 mm: (a) the position of 50 mm away from the gate; (b) the position of 100 mm away from the gate; (c) the position of 150 mm away from the gate; (d) the position of 200 mm away from the gate; and v—vertical to melt flow direction; p—parallel to melt flow direction. [Color figure can be viewed in the online issue, which is available at wileyonlinelibrary.com.]

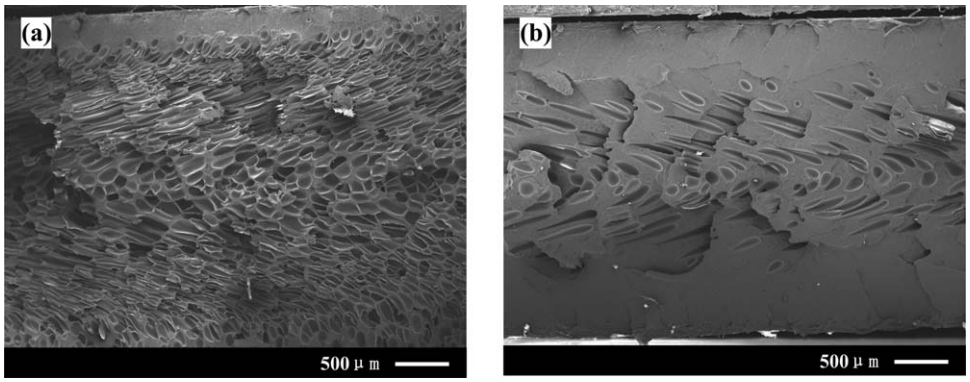

Figure 7. SEM micrographs of the positions of the fractured surface on which the cells begin to distort along the direction parallel to the melt flow direction in the molded parts: (a) shot size of 24 mm, gate position; (b) shot size of 120 mm, position of 300 mm away from the gate.

flow front, it is difficult to distinguish the shape of the cells on the fractured surface, only laminated cells are found in the foamed region as shown in Figure 6(d-p).

The morphology of cell structure in the molded parts with the shot sizes of 24, 48, 96, and 120 mm is similar to that of the part with the shot size of 72 mm. The main difference is that the positions in which the cells on the fractured surfaces parallel to melt flow direction begin to distort are different, for the parts with different shot sizes. The smaller the shot size is, the closer the position of the fractured surface on which the cells begin to distort is to the gate, whereas the larger the shot size is, the further the position of the fractured surface on which the cells begin to distort is from the gate. Figure 7 shows the SEM micrographs of the positions in which the cells on the fractured surface parallel to melt flow direction begin to distort for the shot sizes of 24 and 120 mm, respectively. These two positions correspond to the positions of the gate and 300 mm away from the gate, respectively.

Comparing the cell structures of the microcellular injection-molded parts with different shot sizes, it is found that when the shot size is small, the cell structures in the molded part parallel to melt flow direction are all spindly ellipsoidal cells. Only when the shot size increased to a certain value, the cell structures in the molded part parallel to melt flow direction begin to appear regular near-spherical cells. Figure 8 shows the cell structures of the microcellular injection-molded parts with shot sizes of 24 and 72 mm parallel to melt flow direction. As shown in Figure 8, it can be seen that for the shot size of 24 mm, the

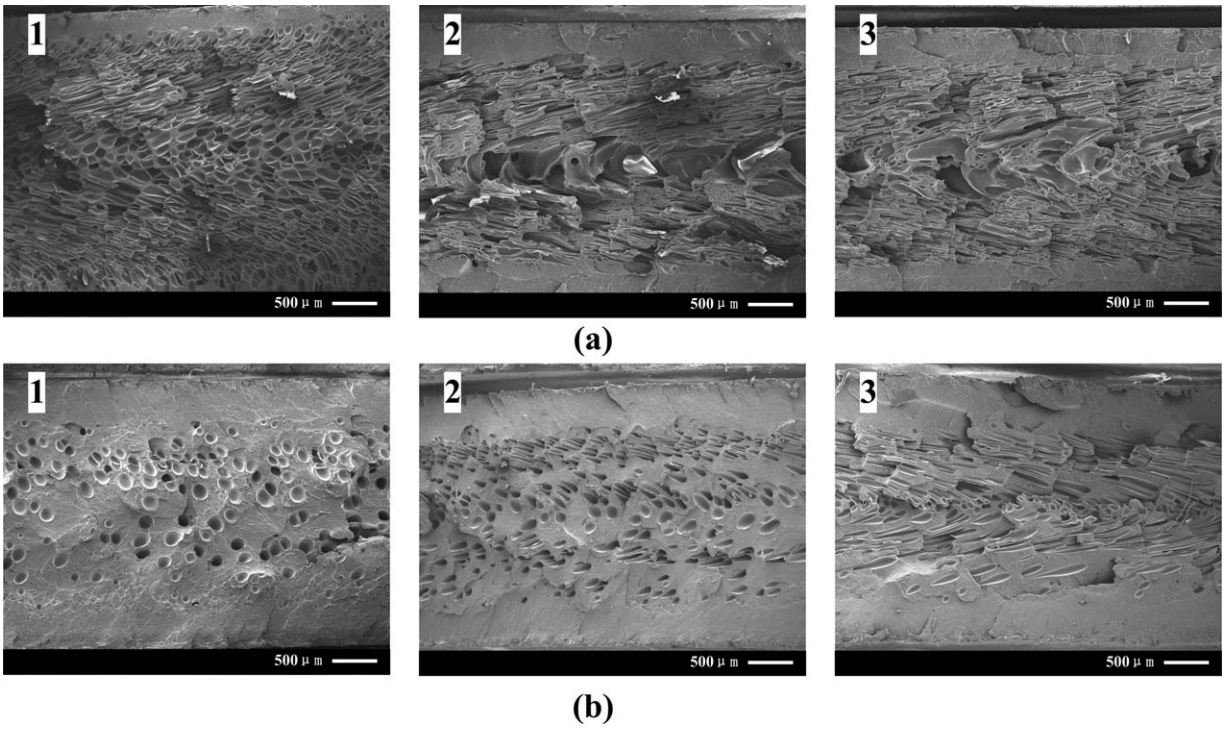

Figure 8. SEM micrographs of the cell structures in the molded parts along the direction parallel to the melt flow direction: (a) shot size of 24 mm; (b) shot size of 72 mm; and 1—gate position; 2—50 mm away from the gate position; 3—100 mm away from the gate position.

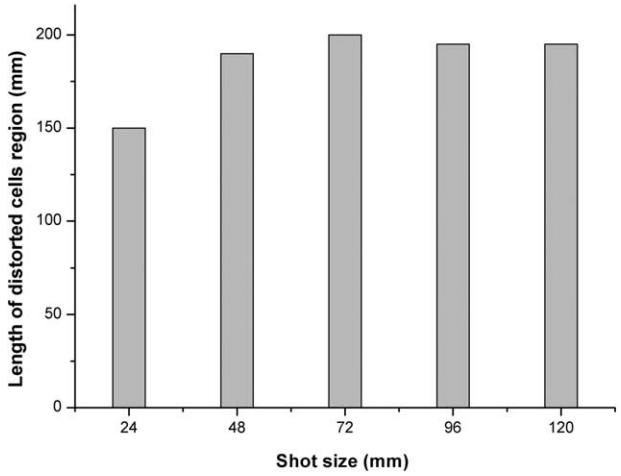

Figure 9. The length of the distorted cells region in the molded parts for different shot sizes.

cells in the molded part parallel to the melt flow direction are all distorted, even in the gate position as shown in Figure 8(a1–3); whereas, for the shot size of 72 mm, parallel to melt flow direction, the most of the cells in the molded part in the positions of the gate and 50 mm away from the gate have been turned into near-spherical cells. But in the position of 100 mm away from the gate, the cells begin to be distorted obviously again as shown in Figure 8(b1–3).

By measuring the dimensions of the distorted cells regions in the molded parts with the shot sizes of 24, 48, 72, 96, and 120 mm, it is obtained that the lengths of the distorted cells region in the molded parts along the melt flow direction are 150, 190, 200, 195, and 195 mm, respectively, as shown in Figure 9. As under the shot size of 24-mm condition, the cells have been distorted from the gate position and there are no obvious boundaries between the regular near-spherical cells and the distorted ellipsoidal cells, and hence the length of the distorted cells region in the molded part cannot represent the actual one. However, for the shot sizes of 48, 72, 96, and 120 mm, there are obvious boundaries between the regular near-spherical cells and the distorted ellipsoidal cells. Therefore, the lengths of the distorted cells region in the molded parts with shot sizes of 48, 72, 96, and 120 mm can be selected as the reference values, and their average value is 195 mm. This indicates that the length of the distorted cells region is 195 mm for the studied part in the experimental conditions of this article.

From the cell morphology of the distorted cells region in microcellular injection-molded parts with different shot sizes, it can also be found that the cell distortion pattern in this region is just corresponded to the fountain-flow behavior of the melt filling in injection stage. We thought that these distorted cells may be caused by the fountain flow of melt filling in mold cavity. In other words, these distorted cells are formed during the filling stage, and their distortions are resulted by the melt flow. On the contrary, the regular near-spherical cells without distortion in the molded part near the gate are formed after the melt filling stage because when the filling stage is just finished the melt has stopped flowing, and hence the cells are not distorted. Therefore, we call these two cell forming processes in microcellular injection molding as "foam during filling" process and "foam after filling" process, respectively.

Cell Formation Mechanism

To verify the two cell forming processes in microcellular injection molding, the cell forming mechanism is analyzed below.

It is known that the solubility of gas in the polymer melt will increase with the increasing pressure,[25] and recently Li et al.[26–29] and Aboozar and Hamid[30] successfully predicted this trend by back propagation artificial neural network based on the self-adaptive particle swarm optimization algorithm and chaos theory. For microcellular injection molding process, in the plasticizing stage, the melt pressure is high and the solubility of the gas is high too, at this moment, the polymer is saturated with the gas blowing agent to form a single-phase polymer–gas solution. When the solution is injected into a mold cavity with low pressure (commonly, atmosphere pressure), the pressure drops quickly, and the gas blowing agent becomes supersaturated within the polymer melt, at this moment, the gas blowing agent will begin to precipitate out in the form of gas, thereby foaming the polymer. However, as the shot size increases in the filling stage, the injection pressure increases, and the melt pressure in the mold cavity increases too. Hence, when the pressure of the melt in the mold cavity increases to a critical value under which the solubility of the gas in the polymer melt is just not supersaturated, at this point, the gas will not precipitate out from the melt yet.

Thus, at the beginning of the melt filling stage of microcellular injection molding, the single-phase polymer–gas solution kept under a high pressure in the barrel is injected into the mold cavity with a low pressure. Once the melt is filled into the mold cavity, the pressure of the melt flow front is dropped rapidly and substantially. This pressure drop causes the solubility of the gas in the polymer melt to reach supersaturated, and a large number of cells are formed. This cell forming process is the "foam during filling" process. Then, when the pressure of the melt behind the melt flow front in the cavity increases to a critical value under which the solubility of the gas in the polymer melt is just not supersaturated, from this moment, there will not be any cell formed in the polymer melt until the filling stage is finished. Once the filling process is finished, the gate is closed and the melt begins to be cooled down. The pressure of the unfoamed melt drops owing to the cooling shrinkage of the melt. Then the solubility of the gas in the polymer melt is supersaturated, the melt foams, and the cells are formed. This cell forming process after the melt filling stage is the "foam after filling" process.

To find out the existence of the critical pressure value of the melt in the mold cavity in filling stage, the melt filling process was numerically simulated by using the software Moldflow. The relationship between the flow length and the melt pressure in the filling stage with shot sizes of 24, 48, 72, 96, and 120 mm was obtained, respectively, as shown in Figure 10.

As shown in Figure 10, it can be found that the melt pressure increases with the increase of the shot size, and the change trends of the melt pressure with the shot sizes along the melt flow direction are basically same. For each shot size, the closer

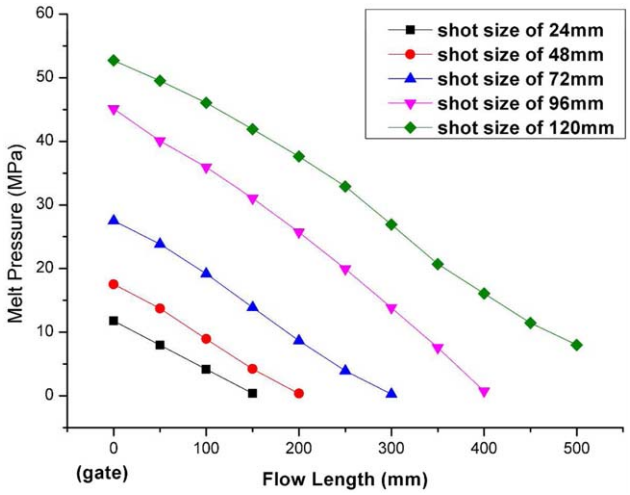

Figure 10. The relationship between the melt pressure and the flow length in the filling stage with the shot sizes of 24, 48, 72, 96, and 120 mm. [Color figure can be viewed in the online issue, which is available at wileyonlinelibrary.com.]

to the gate position the position is, the higher the melt pressure in this position is. Based on the abovementioned analysis, it is known that the average straight length of the distorted cells region in the molded parts formed by the "foam during filling" process is 195 mm away from the melt flow front in this study's conditions. Through numerical simulation of the melt filling process, the melt pressures of the specific position, 195 mm away from the melt flow front, under different shot sizes of 48, 72, 96, and 120 mm are obtained. They are 18.53, 20.65, 21.94, and 22.46 MPa, respectively. The maximum difference between these pressures is 3.93 MPa, and the average value is 20.9 MPa. In the experiments of this study, the pressure of the single-phase polymer–gas solution in the barrel is about 20 MPa. It can be found that the average pressure is almost equivalent to that of the single-phase polymer–gas solution in the barrel. Therefore, this average pressure value can be proposed as the critical melt pressure under which the solubility of the gas in the polymer melt is not supersaturated and melt begins to not foam.

It should be noted that the critical melt pressure under which the melt begins to not foam obtained by the numerical simulation may be slightly higher than the real one. This is because that the polymer material used in numerical simulation is ABS resin and the influence of the dissolved gas on the polymer properties is not considered. In reality, the viscosity of the polymer–gas solution is lower than that of the polymer melt without the dissolved gas, and the real melt pressure is lower than the simulated pressure. Therefore, the real critical pressure value may be lower than 20.9 MPa. It needs further study to determine the actual value of the critical melt pressure, but it does not affect the understanding and analyzing about the cell forming process in this study.

Cell Forming Process

Based on the above analysis and findings, it is concluded that in microcellular injection molding process, the melt foams at the beginning of the filling stage, and the melt pressure increases with the increase of the shot size, when the melt pressure increases to a critical value, the melt will not foam. Hence, there are two regions in the polymer melt filling into the mold cavity which are divided by the critical melt pressure. The melt between the flow front and the position that the critical melt pressure lies in has a pressure lower than the critical value and foams in the filling stage. The melt between the gate and the position that the critical melt pressure lies in has a pressure higher than the critical value and does not foam during the filling stage, but it foams after the filling stage.

Figure 11 shows the schematic representation of the cell forming mechanism in microcellular injection molding process. It is described as follows:

1. At the beginning of filling stage in the microcellular injection molding process, the single-phase polymer–gas solution is injected into the mold cavity with an initial low pressure, the rapid and substantial pressure drop of this solution causes the solubility of the gas in the polymer melt to reach supersaturated, then a large number of cells are formed and the cells near the melt flow front are distorted by the fountain-flow behavior of the melt filling as shown in Figure 11(a).
2. As the shot size increases, the pressure of the melt injected into the mold cavity increases. After the pressure of the melt injected into the mold cavity increases to a critical value, at this moment, the solubility of the gas in the polymer melt is just not supersaturated. The melt newly injected into the mold cavity will not foam. In this way, the melt injected into the mold cavity is divided into two regions by the critical melt pressure as a dividing line as shown in

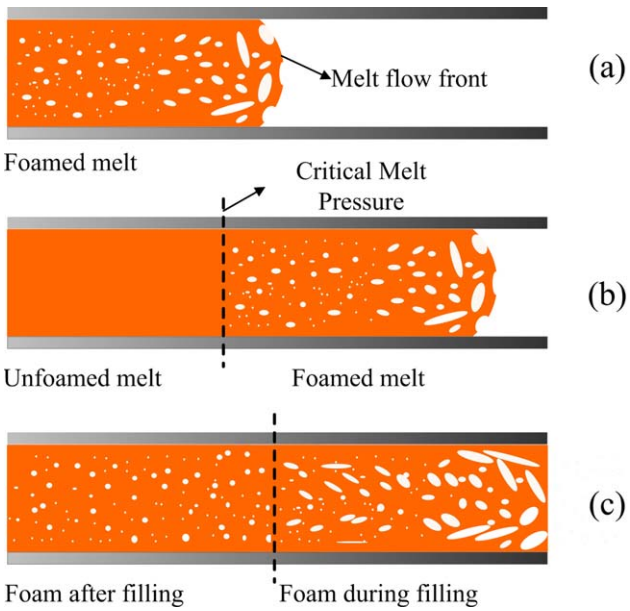

Figure 11. The cell forming process in microcellular injection molding: (a) at the beginning of the filling stage; (b) in the middle of the filling stage; and (c) after the filling stage. [Color figure can be viewed in the online issue, which is available at wileyonlinelibrary.com.]

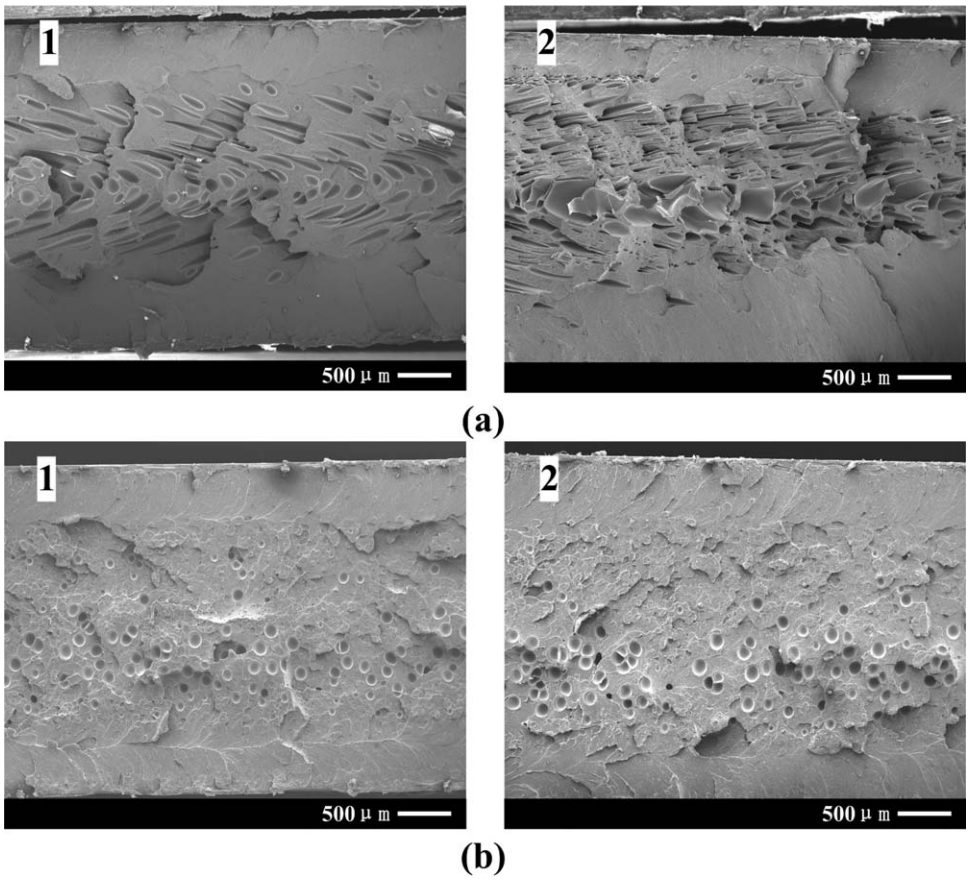

Figure 12. The cell structure of microcellular injection-molded parts along the direction parallel to the melt flow direction for different shot sizes: (a) shot size of 120 mm; (b) shot size of 124 mm; and 1—position of 300 mm away from the gate; 2—position of 350 mm away from the gate.

Figure 11(b). The melt between the flow front and the dividing line has a pressure lower than the critical value and foams in the filling stage, whereas the melt between the gate and the dividing line has a pressure higher than the critical value and does not foam in the filling stage until the filling stage is finished.

3. Once the filling stage is finished, the gate is closed, and the pressure of the melt between the gate and the dividing line drops owing to the cooling shrinkage. This pressure drop causes the solubility of the gas in the polymer melt supersaturated and the melt in this region begins to foam. As the melt in the mold cavity has not yet flowed at this moment, the cells formed in this region have not been distorted. But the previously formed cells in the region between the melt flow front and the dividing line will remain their cell patterns or the distorted cell patterns in the cooling stage as shown in Figure 11(c). Therefore, there are two kinds of cell structures in the microcellular injection-molded parts: the distorted ellipsoidal cells formed in the "foam during filling" process and the regular spherical cells formed in "foam after filling" process.

In addition, it is also found from the experiment that the region with the distorted cells in the molded parts will decrease if further increasing the shot size from 120 mm. The distorted cells formed in "foam during filling" process will gradually evolve into the regular spherical cells formed in "foam after filling" process.

Figure 12 compares the cell structure in the microcellular injection-molded parts along the direction parallel to the melt flow direction with the shot sizes of 120 and 124 mm. It can be seen that, for the shot size of 120 mm, the cells in the positions of 300 and 350 mm away from the gate in the molded part along the direction parallel to the melt flow direction are all distorted cells formed in "foam during filling" process as shown in Figure 12(a-1,a-2). However, when the shot size increases to 124 mm, the cells in the same positions in the molded part along the direction parallel to the melt flow direction have totally evolved into the regular spherical cells formed in "foam after filling" process as shown in Figure 12(b-1,b-2). This may be because that when the shot size increases further, the melt pressure increases too, the cells formed in "foam during filling" process will dissolve into the melt again under a high-pressure condition. After the filling stage is finished, the melt pressure decreases owing to the cooling shrinkage of the melt, the melt foams, and the regular spherical cells are formed again as shown in Figure 12(b-1,b-2).

These two cell forming processes would give a clear understanding of cell structure in former researchers' study. Yuan et al.[19] found that as the weight reduction increases, a high degree of cell shear deformation can be seen in the SEM micrographs

along the melt flow direction, and this phenomena will be easily explained with the principle of cell forming process. As there are two cell forming processes in the microcellular injection molding, when the weight reduction increases, the cells formed in "foam during filling" process will not dissolve into the melt and retain in the part finally.

CONCLUSIONS

In this study, the experiment of microcellular injection-molded parts with different shot sizes was carried out. The cell structures in the molded parts along the direction parallel and vertical to the melt flow direction were both studied. According to the morphology of the cell structure and the melt flow behavior in filling stage, two cell forming processes in microcellular injection molding were proposed. The effects of the shot size and the melt pressure on the cell forming processes were also investigated. The following conclusions were drawn.

1. For the microcellular injection-molded parts with the different shot sizes, there are two kinds of cell structure in the molded parts along the direction parallel to the melt flow direction: the regular spherical cells and the distorted ellipsoidal cells. The deformation pattern of the distorted cells is corresponding to the fountain-flow behavior of the melt in the filling stage. The straight length of the distorted cells region in the molded parts along the melt flow direction basically remains unchanged. Under the experimental conditions of this study, the straight length is 195 mm away from the melt flow front.
2. In the microcellular injection molding process, there are "foam during filling" process and "foam after filling" process, which, respectively, correspond to the final distorted ellipsoidal cells and regular spherical cells in the molded parts. If further increasing the shot size from 120 mm, the region with the distorted cells in the molded parts will decrease, and the distorted cells formed in "foam during filling" process will gradually evolve into the regular spherical cells formed in "foam after filling" process.
3. The melt pressure in the filling stage of the microcellular injection molding process has a dominant effect on the cell forming processes. There exits a critical value of the melt pressure in filling stage. This critical melt pressure divides the melt injected into the mold cavity into two regions. The melt with a pressure lower than the critical pressure will generate "foam during filling" process, and the melt with a pressure higher than the critical pressure will generate "foam after filling" process.

FUTURE WORKS

Owing to the complex structure of the existing mold, it is very difficult to assemble pressure transducers, and hence there is a temporary lack of experimental verification to correlate the numerical results with the real ones. We have begun to design a new injection mold assembled a mold marshalling system to verify the numerical results, and conducting necessary theoretical analysis to establish a cell forming kinetics model related to melt pressure, solubility of gas in polymer, and degree of super saturation.

ACKNOWLEDGMENTS

This research study was supported by Program for Chang Jiang Scholars and Innovative Research Team in University of Ministry of Education of China (No. IRT0931), Research Award Fund for Shandong Province Excellent Innovation Team (No. 2012-136), China Postdoctoral Science Foundation funded project (No. 2012M521329), and Special Fund for Postdoctoral Innovative Project of Shandong Province (No. 201201006).

REFERENCES

1. Martini, J. E.; Waldman, F. A.; Suh, N. P. *SPE Tech. Pap.* **1982**, *28*, 674.
2. Martini, J. E.; Suh, N. P.; Waldman, F. A. *US Pat. 4*, 473,665, **1984**.
3. Kumar, V.; Weller, J. E. *SPE Tech. Pap.* **1992**, *38*, 1508.
4. Baldwin, D. F.; Suh, N. P. *SPE Tech. Pap.* **1992**, *38*, 1503.
5. Gong, W.; Gao, J. C.; Jiang, M.; He, L.; Yu, J.; Zhu, J. H. *J. Appl. Polym. Sci.* **2011**, *122*, 2907.
6. Kumar, V.; Suh, N. P. *Polym. Eng. Sci.* **1990**, *30*, 1323.
7. Baldwin, D. F.; Suh, N. P.; Shimbo, M. *Cell. Polym.* **1992**, *38*, 109.
8. Pilla, S.; Kim, S. G.; Auer, G. K.; Gong, S.; Park, C. B. *Polym. Eng. Sci.* **2009**, *49*, 1653.
9. Adhikary, K. B.; Islam, M. R.; Rizvi, G. M.; Park, C. B. *J. Thermoplast. Compos.* **2013**, *26*, 1127.
10. .Trexel, Inc. Available at: http://www.trexel.com. Accessed on 10 September 2013.
11. Pilla, S.; Kramschuster, A.; Lee, J.; Clemons, C.; Gong, S. Q.; Turng, L. S. *J. Mater. Sci.* **2010**, *45*, 2732.
12. Lee, J.; Turng, L. S.; Dougherty, E.; Gorton, P. *Polym. Eng. Sci.* **2011**, *51*, 2295.
13. Cabrera, E. D.; Mulyana, R.; Castro, J. M.; Lee, L. J.; Min, Y. *J. Appl. Polym. Sci.* **2013**, *127*, 3760.
14. Lee J. J.; Cha S. W. *Cell. Polym.* **2005**, *24*, 279.
15. Gong, W.; Gao, J. C.; Jiang, M.; He, L.; Yu, J.; Zhu, J. H. *J. Appl. Polym. Sci.* **2011**, *122*, 2907.
16. Jeon, B.; Han, J. W.; Lee, K. S.; Cha, S. W. *Polym. Plast. Technol. Eng.* **2012**, *51*, 401.
17. Behravesh, A. H.; Rajabpour, M. *Cell. Polym.* **2006**, *25*, 85.
18. Yuan, M. J.; Turng, L. S.; Gong, S. Q.; Caulfield, D.; Hunt, C.; Spindler, R. *Polym. Eng. Sci.* **2004**, *44*, 673.
19. Rezavand, S. A. M.; Behravesh, A. H.; Mahmoodi, M.; Shahi, P. *Cell. Polym.* **2009**, *28*, 405.
20. Hwang, S. S.; Liu, S. P.; Hsu, P. P.; Yeh, J. M.; Yang, J. P.; Chang, K. C.; Chu, S. N. *Int. J. Heat Mass Transfer* **2011**, *38*, 597.
21. Hwang, S. S.; Liu, S. P.; Hsu, P. P.; Yeh, J. M.; Yang, J. P.; Chen, C. L. *Int. J. Heat Mass Transfer* **2012**, *39*, 383.
22. Leicher, S.; Walter, A.; Schneebauer, M.; Wagner, M.; Kopp, T.; Wintermantel, E. *Cell. Polym.* **2006**, *25*, 99.

23. Huang, H. X.; Wang, J. K. *Polym. Test.* **2008**, *27*, 513.
24. Gomez-Gomez, J. F.; Arencon, D.; Sanchez-Soto, M. A.; Martinez, A. B. *J. Cell. Plast.* **2013**, *49*, 47.
25. Xu, J. Y. *Microcellular Injection Molding*, Wiley Series on Polymer Engineering and Technology; Hoboken, New Jersey, **2010**.
26. Li, M. S.; Huang, X. Y.; Liu, H. S.; Liu, B. X.; Wu, Y.; Xiong, A. H.; Dong, T. W. *Fluid Phase Equilibr.* **2013**, *356*, 11.
27. Li, M. S.; Huang, X. Y.; Liu, H. S.; Liu, B. X.; Wu, Y. *J. Appl. Polym. Sci.* **2013**, *130*, 3825.
28. Li, M. S.; Huang, X. Y.; Liu, H. S.; Liu, B. X.; Wu, Y.; Ai, F. R. *Acta Chim. Sinica.* **2013**, *71*, 1053..
29. Li, M. S.; Huang, X. Y.; Liu, H. S.; Liu, B. X.; Wu, Y.; Deng, X. Z. *J. Appl. Polym. Sci.* **2013**, *129*, 3297.
30. Aboozar, K.; Hamid, M. *Expert Syst. Appl.* **2010**, *37*, 3070.